Initiation and Propagation of Spectrin Heterodimer Assembly Involves Distinct Energetic Processes†

Donghai Li, Sandra Harper, and David W. Speicher*

The Wistar Institute, Philadelphia, Pennsylvania 19104

Received April 26, 2007; Revised Manuscript Received July 9, 2007

ABSTRACT: Red cell spectrin α and *β* subunits consist primarily of many tandem homologous motifs with very similar three- helix-bundle structures and similar dimer interfaces. Although misassembled homodimers can form under some conditions, correctly aligned heterodimers consistently assemble provided a small "dimer initiation" site near the actin binding domain is present. The dimer initiation site has been characterized to some extent, but little is known about the subsequent, low-affinity lateral interactions of the remaining motifs along the length of this ropelike molecule or the forces involved in these two steps of the dimerization process. In this study, we used isothermal titration calorimetry to deduce the mechanism and energetics of the two heterodimer assembly phases. The high-affinity initiation of dimerization is primarily enthalpically driven, which is consistent with initial alignment and docking of specific complementary α and *β* motifs in the dimer initiation site driven by long-range electrostatic interactions followed by tight binding stabilized by hydrogen bonds and other hydrophilic interactions. In contrast, the subsequent weak lateral associations of additional motifs are primarily entropically driven, suggesting binding primarily involves weak hydrophobic interactions. Although initial docking is largely electrostatic, the only lateral interaction within the first four pairs of motifs that involves a net change in protons is the interaction of the α18 and *β*4 repeats. This substoichiometric uptake of protons could be due to a pK_a shift of a histidine in the α18 motif located near the dimer interface in a proposed homology-based model. On the basis of this analysis of heterodimer thermodynamics, a detailed model of spectrin dimer assembly is proposed.

Erythrocyte spectrin, a major component of the membrane skeleton that contributes to both the stability and the elasticity of the red cell membrane, was first discovered as the principal protein in low-ionic-strength extracts of erythrocyte membranes (*1*−*3*). The basic functional unit of spectrin is a heterodimer, which forms a flexible 100 nm rodlike structure by side-to-side, antiparallel association of a ∼280 kDa α subunit with a ∼246 kDa *β* subunit as visualized by electron microscopy (*4*). The spectrin heterodimer is comprised primarily of many tandem homologous 106-residue "spectrin-type" motifs (*5*), which are sometimes called "spectrin repeats". These homologous motifs are primarily comprised of three helix bundles, i.e., helices A, B, and C (*6*). The α subunit contains 20 such motifs, an SH3 domain (α10), C-terminal EF hand motifs, and an N-terminal partial motif consisting of a single C helix. The *β* subunit contains 16 full motifs, a partial 17th motif (the A and B helices), an N-terminal actin binding domain (ABD), and a C-terminal domain that contains six phosphorylation sites (*7*). A schematic of the spectrin dimer motif structure is shown in Figure 1A. Spectrin heterodimers further associate in a head-to-head orientation to form 200 nm long tetramers, the predominant form of spectrin in the red cell membrane skeleton.

Lateral assembly of the spectrin α and *β* chains was previously proposed to occur in a zipperlike fashion, beginning with a dimer initiation site located near the actin binding end of the molecule (*8*). Consistent with the critical role of these motifs in dimerization, a very common low-expression polymorphism called α^{LELY}, which contains two coding region mutations, a Leu → Val mutation at codon 1857 and a 50% skipping of exon 46, which encodes six amino acids (residues 2177−2182), can result (*9*). We previously showed that the Leu → Val substitution did not affect incorporation of α subunits into dimers and hence into red cell membranes, but the deletion of the six amino acids encoded by exon 46 prevented these subunits from being incorporated into the membrane (*10*). Dimerization studies of α and *β* chains using an HPLC gel filtration binding assay and recombinant spectrin peptides demonstrated that the α20−21 and *β*1−2 regions comprise the minimum initiation site required for initial high-affinity lateral association (*11*). Furthermore, a subsequent study using titration calorimetry and pull-down assays convincingly demonstrated the adjacent terminal nonhomologous domains (ABD and EF hand motifs) do not significantly contribute to heterodimerization (*12*). These results were in contrast to a study using immunoprecipitation assays to study heterodimer assembly of *Drosophila* spectrin,

† This work was supported by NIH Grant HL38794 to D.W.S. and by institutional grants to the Wistar Institute including an NCI Cancer Core Grant (CA10815) and the Commonwealth Universal Research Enhancement Program, Pennsylvania Department of Health.

* To whom correspondence should be addressed: Phone: (215) 898-3972. Fax: (215) 898-0664. E-mail: speicher@wistar.org.

10.1021/bi7007905 CCC: $37.00
Published on Web 08/22/2007

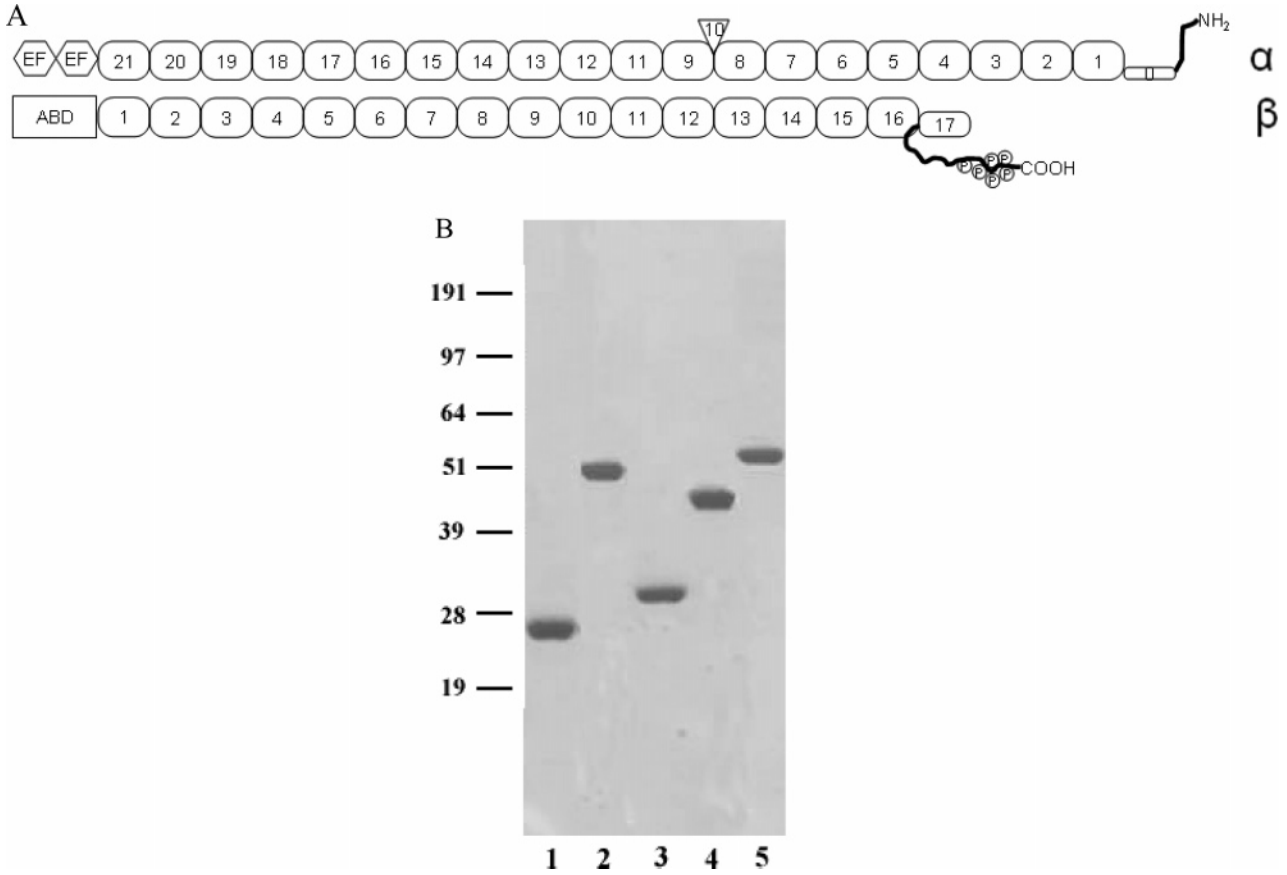

FIGURE 1: Model of spectrin motifs. (A) The structural motifs in an antiparallel red cell spectrin heterodimer are schematically represented as follows: numbered rounded rectangles, homologous spectrin motifs or repeats numbered from the N- to C-terminal; triangle, SH3 domain originally labeled as the α10 motif; hexagons, EF hand regions; large rectangle, actin binding domain. α0 represents a partial motif at the N-terminus of the α spectrin. The "tail" at the C-terminal end of the β spectrin extending from the partial β17 motif is the nonhomologous phosphorylated region. (B) SDS gel of the purified recombinants used in this study. Each lane contains 2 μg of purified protein. Key: lane 1, α20−21; lane 2, α18−21; lane 3, β1−2; lane 4, β1−3; lane 5, β1−4.

which suggested these adjacent nonhomologous domains were needed for heterodimer formation of the *Drosophila* isoform (*13*, *14*).

Molecular models of the dimer initiation region suggested that docking of the correct α and β motifs involved interactions of complementary electrostatic surfaces (*15*). Interestingly, these heterodimer interactions result in coupled unfolding of the laterally associated α and β motifs when dimeric recombinants are unfolded under tensile stress using atomic force microscopy (*16*). Other studies showed that α-spectrin is ubiquitinated in repeats α20 and α21, although these modifications do not appear to affect spectrin heterodimer formation. Interestingly, a marked reduction of red blood cell spectrin ubiquitination is observed in homozygous sickle cell patients (*17*−*20*). Crystallographic structures are now available for a one-motif *Drosophila* α-spectrin fragment (*6*), two- and three-motif fragments of chicken brain α-spectrin (*21*, *22*), two-motif fragments of human erythroid β-spectrin (*23*), and the four-motif human skeletal muscle α-actinin dimerization domain (*24*, *25*). However, so far, attempts to produce crystal structures of the spectrin dimer initiation site have been unsuccessful. Hence, one of the most efficient ways to gain further insight into detailed properties of the protein−protein interactions for this critical spectrin assembly process is through characterization of binding energetics and correlation of the assembly energetics with molecular interactions implicated in the two phases of dimer assembly.

In the present study, we used isothermal titration calorimetry to investigate the thermodynamic properties of spectrin heterodimerization using α- and β-spectrin recombinant peptides of differing lengths (α20−21, α18−21, β1−2, β1−3, and β1−4). The two phases of dimerization have distinct energetics indicative of quite different interacting surfaces. The association of the dimer initiation site motifs is primarily enthalpically driven, indicating this interaction is probably stabilized primarily by hydrogen bonds and other hydrophilic interactions. Subsequent weak lateral associations of adjacent motifs are primarily entropically driven and apparently predominantly involve weak hydrophobic interactions that are sufficient to keep the chains laterally paired under physiological conditions. These additional associations provide only subtle contributions to the overall heterodimer affinity.

MATERIALS AND METHODS

Construction of Expression Plasmids. The following recombinant peptides were used in this study: α20−21 (motifs 20 and 21 of the α subunit, comprising residues 2033−2259), α18−21 (motifs 18−21, residues 1818−2259), β1−2 (motifs 1 and 2 of the β subunit, residues 293−528), β1−3 (motifs 1−3, residues 293−637), and β1−4 (motifs

1−4, residues 293−743). The motifs described here are structural motifs using the motif start and stop sites described by Yan et al. (*6*) except for the β1 N-terminal start site, which was defined by Ursitti et al. (*11*). The design and construction of the α20−21, α18−21, β1−2, β1−3, and β1−4 pGEX-2T expression plasmids were previously described (*11*).

Expression and Purification of Recombinant Erythrocyte Spectrin Peptides. The spectrin−GST[1] fusion proteins were expressed and purified as described (*11*, *15*), except that β1−2, β1−3, β1−4, and α18−21 were expressed at 30 °C, α20−21 was expressed at 18 °C, and all of the proteins were purified from the soluble fraction after cell lysis. Peptides were cleaved from the GST molecule using bovine thrombin (Sigma) at 37 °C for 3 h. NaCl was added to varying final concentrations depending on the recombinant protein to decrease the formation of secondary cleavage products during thrombin cleavage. The cleaved spectrin peptides were purified by rechromatography on a glutathione−Sepharose column. The α20−21 peptide was further purified from residual GST by anion-exchange chromatography on a 1 mL HiTrap-Q column (GE Healthcare). The α20−21 peptide was bound to the column in buffer A (65 mM NaCl, 5 mM sodium phosphate, 2.5 mM EDTA, 75 μM PMSF, pH 7.3), washed with buffer A, and eluted with buffer B (1 M NaCl, 5 mM sodium phosphate, 2.5 mM EDTA, 75 μM PMSF, pH 7.3). The final purification step for all spectrin peptides was HPLC gel filtration on two preparative TSK-gel columns (G3000SW + G2000SW) in series in phosphate-buffered saline (10 mM sodium phosphate, 130 mM NaCl, 1 mM EDTA, 0.15 mM PMSF, 1 mM β-mercaptoethanol, pH 7.4).

Polyacrylamide Gel Electrophoresis. SDS−polyacrylamide gel electrophoresis was performed using 12% NuPAGE Bis-Tris gel with MOPS running buffer (Invitrogen). All gels were stained with Coomassie Brilliant Blue R-250.

Differential Scanning Calorimetry (DSC). DSC measurements were preformed using a MicroCal MCS calorimeter. All protein solutions were exhaustively dialyzed against 10 mM sodium phosphate, 130 mM sodium chloride, 1 mM 2-ME, pH 7.4. Prior to being loaded into the calorimeter, the samples were degassed for 5 min. An aliquot of the dialysate was used in the reference cell. The protein concentration was between 0.5 and 1.1 mg/mL. All scans were performed from 10 to 90 °C using a scan rate of 90 °C/h. ORIGIN software provided with the instrument was used for data analysis. Briefly, a buffer blank was subtracted from the raw experimental data, and then a baseline was defined using the progress curve function fitted to the end points of the transition. The constructed baseline was then subtracted, and the data were curve fitted using standard models to determine T_m associated with the unfolding.

Isothermal Titration Calorimetry. Isothermal titration calorimetry experiments were performed using a MicroCal VP-ITC instrument equilibrated at 30 °C. Samples for titration calorimetry were dialyzed against 10 mM sodium phosphate, 130 mM NaCl, 1 mM β-mercaptoethanol, pH 7.4 (or 20 mM TrisCl, 130 mM NaCl, 1 mM TCEP, pH 7.4, or 20 mM HEPES, 130 mM NaCl, 1 mM TCEP, pH 7.4). All solutions were thoroughly degassed before use by stirring under vacuum. Titration was carried out using a 250 μL syringe filled with α20−21 or α18−21 solution (pH 7.4), with stirring at 400 rpm. The concentrations of α20−21 or α18−21 were varied between 30 and 90 μM. Injections were started after baseline stability had been achieved. A titration experiment consisted of an initial injection of 1 μL followed by 22 consecutive injections of 10 μL volume each and with either 5 or 10 min intervals between injections. Calorimetric data were analyzed using MicroCal ORIGIN software. The enthalpy change for each injection was calculated by integrating the area under the peaks and then subtracting the control titration. Titration curves were fitted by a nonlinear least-squares method to a function for the binding of ligand to a macromolecule (*26*). From the curve thus fitted, the parameters ΔH (reaction enthalpy), K_a (binding constant, $K_a = 1/K_d$), and n (reaction stoichiometry) were determined. From the values of K_a and ΔH, the changes in free energy (ΔG) and in entropy (ΔS) were calculated with the equation $\Delta G = -RT \ln K_a = \Delta H - T\Delta S$, where R is the universal molar gas constant and T is the absolute temperature.

Construction of a Homology Model of the α18/β4 Heterodimer. A suitable template (chicken brain spectrin α15−17, PDB ID 1U4Q) for modeling the α18/β4 heterodimer was found via SWISS-MODEL WORKSPACE tools ("Template Identification") (*27*) and MODELLER (*28*). Sequence alignments were produced with CLUSTAL W-1.83 (*29*). The homology model of the α18 and β4 motifs was carried out by sequence alignment of α18/β4 with chicken brain spectrin α15−17. The antiparallel dimer was constructed by application of structural superimposition of target proteins with the crystal structure of chicken brain α15 and α17 heterodimer. Modeling, structural superimposition, and optimization were performed with MODELLER. The most reliable structure was chosen by PROCHECK (*30*), WhatCheck (*27*), and MODELLER DOPE (discrete optimized protein energy) analysis. Molecular graphics were illustrated using PyMol (*31*).

RESULTS

Purification and Characterization of Spectrin Recombinant Peptides. In the current study we used ITC to obtain insight into the mechanisms involved in the two distinct phases of spectrin heterodimer assembly by comparing thermodynamic properties of dimerization using a series of recombinant α (α20−21, α18−21) and β (β1−2, β1−3, and β1−4) peptides. The locations of these recombinants within the overall motif structure of a spectrin heterodimer are shown in Figure 1A, and the purified peptides are shown in Figure 1B. Protein integrity was confirmed by MALDI MS, and potential irreversible aggregation of purified samples was measured shortly before calorimetric measurements using analytical HPLC gel filtration (data not shown). These results together with prior characterization of these recombinants using CD, sedimentation equilibrium, and atomic force microscopy provided assurance these recombinant proteins were properly folded (*11*, *12*, *16*). In addition, these recombinants were analyzed by differential scanning calorimetry, which revealed a single endothermic peak for each construct with the exception of β1−3, where two transitions were observed. The temperatures at the midpoints of the

[1] Abbreviations: GST, glutathione *S*-transferase; EDTA, ethylenediaminetetraacetic acid; PMSF, phenylmethanesulfonyl fluoride; TCEP, tris(2-carboxyethyl)phosphine hydrochloride; HPLC, high-performance liquid chromatography; MALDI MS, matrix-assisted laser desorption/ionization mass spectrometry; DSC, differential scanning calorimetry; ITC, isothermal titration calorimetry.

Table 1: Thermal Unfolding of Spectrin Initiation Site Peptides

protein segment	T_m (°C)	protein segment	T_m (°C)
α20−21	45.0	β1−3[a]	(39.7) 46.4
α18−21	45.8	β1−4	44.5
β1−2	49.2		

[a] This recombinant exhibited two transitions.

thermal unfolding transitions (T_m) are shown in Table 1. As with most spectrin peptides, thermal unfolding was irreversible with extensive precipitation upon unfolding. Hence, it was not practical to estimate the heat capacity, and the T_m values as well as enthalpies should be regarded as approximate. Nonetheless, the high, similar T_m values and estimated enthalpies of unfolding (data not shown) are indicative of well-folded proteins.

Binding Affinity of Varying Length Recombinant Peptides Containing the Dimer Initiation Site. Six heterodimer combinations were analyzed by associating the two-, three-, or four-motif β recombinant with either the two- or four-motif α recombinant (Figure 2). All combinations contained the minimum high-affinity dimer binding site, while the number of unpaired and paired adjacent weakly interacting motifs varied. Initial titrations were conducted using phosphate-buffered saline, pH 7.4, at 30 °C (Figure 3). The binding isotherms for all reactions in phosphate buffer are charac-

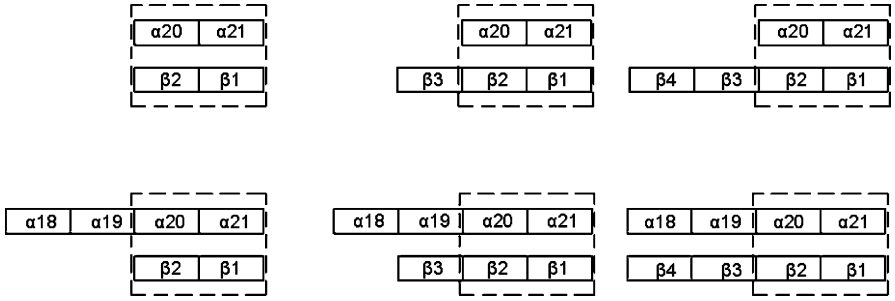

FIGURE 2: Schematic illustrating $\alpha\beta$ dimer combinations. The high-affinity minimum dimer initiation site is enclosed by a dashed box to highlight the number of paired and unpaired weakly interacting motifs in each condition.

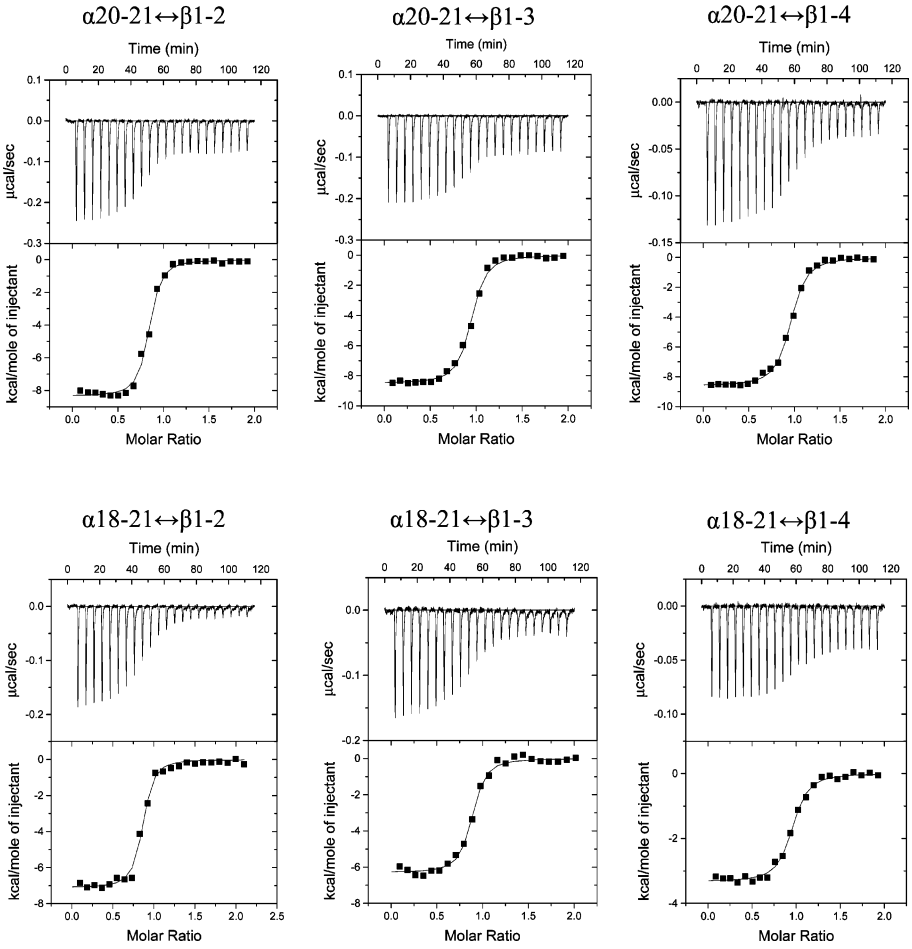

FIGURE 3: ITC data for the binding of α- and β-spectrin recombinants in phosphate buffer, pH 7.4. The concentrations were as follow: α20−21 (64.2 μM) + β1−2 (5.5 μM), α20−21 (43.9 μM) + β1−3 (3.7 μM), α20−21 (32.2 μM) + β1−4 (2.8 μM), α18−21 (68.8 μM) + β1−2 (5.4 μM), α18−21 (46.0 μM) + β1−3 (3.8 μM), α18−21 (33.2 μM) + β1−4 (2.8 μM). Upper panels: ITC thermographs. Lower panels: fitted binding isotherms. In all cases, the α recombinant was the titrant and the buffer was 10 mM sodium phosphate, 130 mM NaCl, 1 mM β-mercaptoethanol, pH 7.4.

Table 2: Isothermal Titration Calorimetry Data for Dimerization of α- and β-Spectrin Recombinants[a]

complex	pH	buffer	N^b	K_d (nM)	ΔG_{obsd} (kcal/mol)	ΔH_{obsd} (kcal/mol)	ΔS_{obsd} (cal/(mol K))
α20−21/β1−2	7.4	Phos/2-ME	0.81	27.8	−10.5	−8.4	7.0
α20−21/β1−3	7.4	Phos/2-ME	0.91	24.8	−10.5	−8.5	6.7
α20−21/β1−4	7.4	Phose/2-ME	0.93	21.6	−10.6	−8.6	6.7
α18−21/β1−2	7.4	Phos/2-ME	0.83	27.9	−10.5	−7.1	11.1
α18−21/β1−3	7.4	Phos/2-ME	0.85	23.5	−10.6	−6.3	14.1
α18−21/β1−4	7.4	Phos/2-ME	0.93 ± 0.01	24.0 ± 0.1	−10.6 ± 0.1	−3.2 ± 0.1	24.3 ± 0.1
α20−21/β1−2	7.4	Tris−Cl/TCEP	0.87	21.4	−10.6	−8.7	6.4
α20−21/β1−3	7.4	Tris−Cl/TCEP	0.83	7.8	−11.2	−9.3	6.3
α20−21/β1−4	7.4	Tris−Cl/TCEP	0.87	11.8	−11.3	−9.3	6.7
α18−21/β1−2	7.4	Tris−Cl/TCEP	0.82	29.5	−10.4	−8.2	7.3
α18−21/β1−3	7.4	Tris−Cl/TCEP	0.88	26.7	−10.5	−7.2	10.8
α18−21/β1−4	7.4	Tris−Cl/TCEP	1.06 ± 0.02	15.6 ± 0.1	−10.8 ± 0.1	1.1 ± 0.1	39.2 ± 0.1
α18−21/β1−4	7.4	HEPES/TCEP	0.92	8.7	−11.2	−1.4	32.3
α18−21/β1−4	8.0	Phos/TCEP	1.01	28.4	−10.5	−3.3	23.7
α18−21/β1−4	8.0	HEPES/TCEP	1.02	15.2	−10.8	−2.4	27.8
α18−21/β1−4	8.0	Tris−Cl/TCEP	0.92	8.1	−11.2	−1.0	33.6

[a] Averages and standard deviations are reported for experiments that were performed in duplicate. Other values were from single determinations. The concentration of reducing reagent used in these experiments was 1 mM. [b] N = stoichiometry.

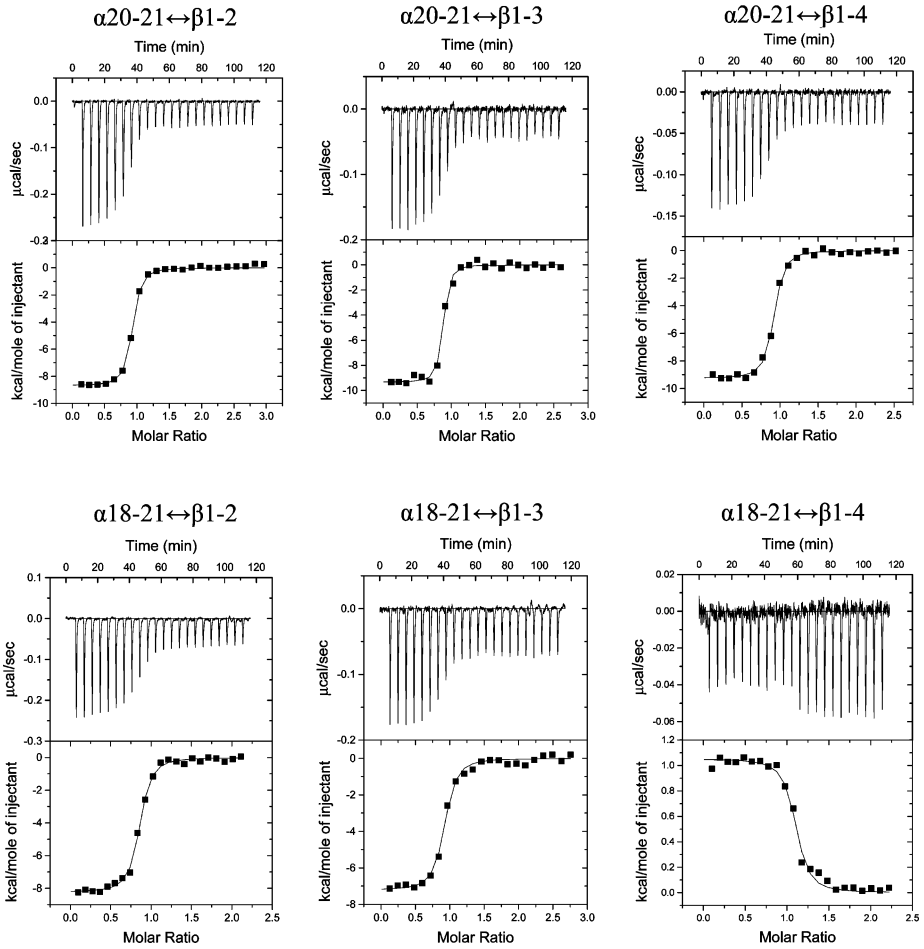

FIGURE 4: ITC data for the binding of α- and β-spectrin recombinants in Tris buffer, pH 7.4. The concentrations were as follows: α20−21 (88.2 μM) + β1−2 (4.9 μM), α20−21 (53.5 μM) + β1−3 (3.4 μM), α20−21 (38.2 μM) + β1−4 (2.5 μM), α18−21 (62.7 μM) + β1−2 (4.9 μM), α18−21 (55.1 μM) + β1−3 (3.3 μM), α18−21 (36.3 μM) + β1−4 (2.7 μM). Upper panels: ITC thermographs. Lower panels: fitted binding isotherms. In all cases, the α recombinant was the titrant and the buffer was 20 mM Tris, 130 mM NaCl, 1 mM TCEP, pH 7.4.

teristic of an exothermic single binding site interaction. Thermodynamic parameters were calculated from fitted isotherms (Table 2), and all interactions showed similar tight interactions with $K_d \approx 25$ nM, indicating the presence of one or two paired or unpaired motifs outside the high-affinity site had no detectable effect on the overall binding affinity. The injection of α20−21 into the suspension of β1−2, β1−3, or β1−4 released heats of reaction (ΔH_{obsd}) of ~8.5 kcal/mol in phosphate buffer, indicating no appreciable contribution of the unpaired β motifs to the heat of reaction. In contrast, the ΔH_{obsd} for interaction of α18−21 with different length β-spectrin recombinants in phosphate-buffered saline

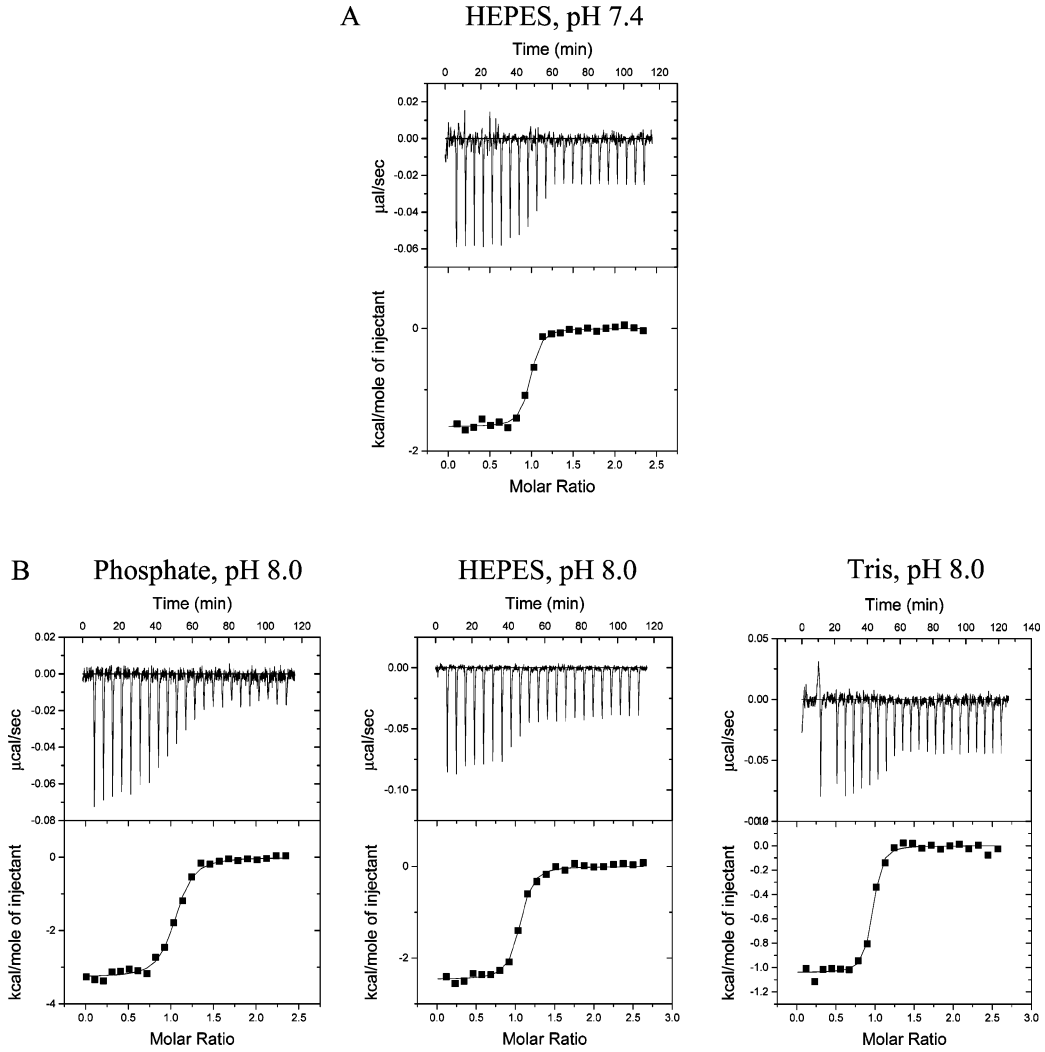

FIGURE 5: Effect of pH on the dimerization of α18−21 and β1−4: (A) 36.9 μM α18−21 + 2.6 μM β1−4 in HEPES buffer, pH 7.4; (B) phosphate, 38.4 μM α18−21 + 2.7 μM β1−4; HEPES, 41.4 μM α18−21 + 2.6 μM β1−4; Tris, 40.5 μM α18−21 + 2.6 μM β1−4. Upper panels: ITC thermographs. Lower panels: fitted binding isotherms.

decreased as low-affinity interactions outside the dimer initiation site occurred, with the most dramatic decrease (∼4 kcal/mol) resulting from lateral association of the fourth pair of motifs (α18 and β4).

Effects of Buffer Ionization and pH on the Binding Enthalpy. The observed enthalpy comprises both the enthalpy of the binding reaction, ΔH_{int}, and the enthalpy associated with the ionization of the buffer caused by any net uptake or release of protons during the reaction, as described in the relationship

$$\Delta H_{obsd} = n_{H^+}\Delta H_{ion} + \Delta H_{int}$$

where n_{H^+} is the number of protons that are transferred from the buffer to the protein upon binding. To test for possible involvement of protons in the binding process, additional titrations for the six α and β combinations were performed in Tris buffer at pH 7.4 (Figure 4), which has an enthalpy of ionization of 11.3 kcal/mol (*32*). All isotherms were similar to those obtained with phosphate buffer with the exception of the α18−21 ↔ β1−4 association, where an exothermic reaction in phosphate buffer became weakly endothermic in Tris buffer, indicating a net uptake of protons during binding of these two four-motif recombinants. The

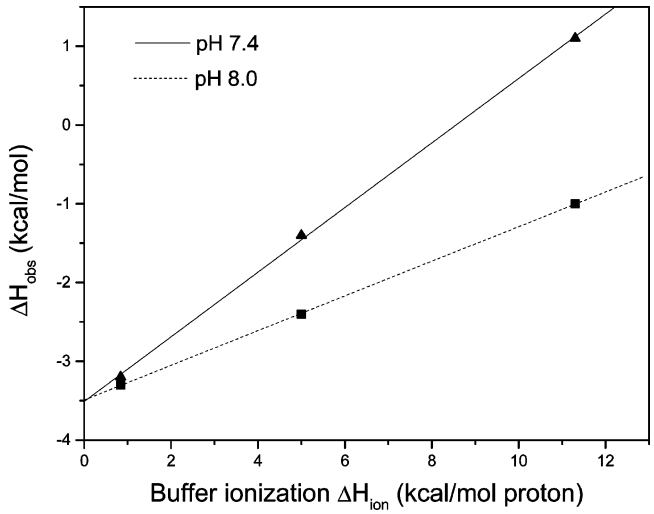

FIGURE 6: Relationship between the observed binding enthalpy and the heat of buffer protonation for dimerization of α18−21 and β1−4. Measurements were made using phosphate (ΔH_{ion} = 0.84 kcal/mol), HEPES (ΔH_{ion} = 5.0 kcal/mol), or Tris (ΔH_{ion} = 11.3 kcal/mol) buffer at pH 7.4 (solid line) and pH 8.0 (dashed line).

thermodynamic parameters were calculated from fitted isotherms (Table 2). Comparisons of observed enthalpy

Table 3: Protonation/Deprotonation Properties

complex	pH	n_{H^+}	complex	pH	n_{H^+}
α20−21/β1−2	7.4	−0.03	α18−21/β1−3	7.4	−0.09
α20−21/β1−3	7.4	−0.08	α18−21/β1−4	7.4	+0.41
α20−21/β1−4	7.4	−0.07	α18−21/β1−4	8.0	+0.22
α18−21/β1−2	7.4	−0.11			

Table 4: Intrinsic Thermodynamic Parameters for Dimerization of α- and β- Spectrin Recombinants

complex	ΔG_{int} (kcal/mol)	ΔH_{int} (kcal/mol)	$-T\Delta S_{int}$ (kcal/mol)
α20−21/β1−2	−10.55	−8.55	−2.00
α20−21/β1−3	−10.89	−8.9	−1.99
α20−21/β1−4	−10.81	−8.95	−1.86
α18−21/β1−2	−10.45	−7.65	−2.80
α18−21/β1−3	−10.54	−6.75	−3.79
α18−21/β1−4	−10.80	−3.51	−7.29

values for the same binding partners in the two different buffers showed the largest change for α18−21/β1−4, where ΔH_{obsd} in Tris buffer increased by +4.3 kcal/mol relative to that in phosphate buffer, while ΔH_{obsd} for the other combinations was relatively unaffected.

The proton effect on the α18−21 ↔ β1−4 interaction was further explored using a third buffer with an intermediate heat of protonation (HEPES) at pH 7.4. As shown in Table 3, the n_{H^+} value for association of α18−21 and β1−4 at pH 7.4 is 0.41. The simplest explanation for this substoichiometric protonation change is the partial uptake of a proton at a single site upon dimerization. This interaction was reanalyzed using the same three buffers at pH 8.0 (Figure 5 and Table 2). The similar dissociation constants observed at pH 8.0 and 7.4 for each buffer demonstrated that this interaction is relatively insensitive to the modest pH change used here. Of course, the pH range that could be surveyed was limited by the pH stability of both the interaction and the individual recombinants. The ΔH_{obsd} values for α18−21 ↔ β1−4 in different buffers were linearly related to the heats of buffer ionization, indicative of a net gain of protons upon dimer assembly for the four-motif recombinants (Figure 6). As indicated by the above equation, in these plots, slope $= n_{H^+}$. Similar plots for other α/β combinations (data not shown) allowed us to estimate the number of protons involved in each reaction (Table 3). These data show no significant net proton uptake or loss is involved in pairing of the first three α/β motifs, while a substoichiometric uptake of a proton is involved in the α18 ↔ β4 association.

The substoichiometric uptake and pH dependency of the number of protons involved in the α18 ↔ β4 association suggest that the p*K* of an ionizable side chain is conformationally affected by dimerization. Assuming a single amino acid residue is involved, the change in the number of protons released or taken up at a binding interface depends upon the proton binding constants and experimental pH as defined by the relationship (*33*)

$$n_{H^+} = \frac{K_p^c \times 10^{-pH}}{1 + K_p^c \times 10^{-pH}} - \frac{K_p^f \times 10^{-pH}}{1 + K_p^f \times 10^{-pH}}$$

where K_p^c and K_p^f are the proton binding constants for the complex and free forms, and the proton binding constants are equal to 10^{pK_a} for the ionizing group. In principle, the determination of n_{H^+} at two different pH values should suffice to calculate the pK_a of the ionizing group in both free and complex forms. On the basis of the n_{H^+} values obtained at pH 7.4 and 8.0 for the binding of α18−21 to β1−4, pK_f and pK_b were determined to be 6.78 and 7.58, respectively. This pK_a change between the free and bound forms is consistent with the uptake of protons when α18−21 is bound to β1−4 and is most likely indicative of a histidine residue or an α-amino group, i.e., the amino terminal of the α18 motif.

DISCUSSION

In the present study, we evaluated the relative thermodynamic contributions to spectrin heterodimer formation of the two distinct assembly phases, i.e., initial high-affinity binding of the dimer initiation site and subsequent lateral low-affinity pairing of additional α and β motifs. Biomolecular equilibrium processes such as spectrin dimerization are governed by free energy changes (ΔG) with reactions involving reduction in free energy (ΔG negative) being favored. The ΔG_{obsd} and corresponding observed entropy change (ΔS_{obsd}) for each α/β combination can be calculated from the experimentally determined ΔH_{obsd} and K_d values (Table 2). As expected, all reactions show large, similar negative ΔG_{obsd} values, indicating dimerization is strongly favored. While the free energy for each combination is similar, the enthalpic (ΔH_{obsd}) and entropic ($-T\Delta S_{obsd}$) contributions to the free energy of dimerization vary substantially depending upon the number of low-affinity motif pairs that can form. Titrations of α18−21 into β1−4 in phosphate, HEPES, and Tris buffers yielded dissociation constants of 24.0, 8.7, and 15.6 nM, respectively, for an average $K_d = 16.1$ nM. Hence, the buffer effect on K_d for α18−21/β1−4 is minor as all K_d values are within 2-fold of the average value, and therefore, the dissociation constant can be used to estimate ΔG_{int} ($\Delta G_{int} = -RT \ln K_d^{-1}$). We can subsequently calculate ΔS_{int} and the contribution of the intrinsic entropy change to ΔG_{int} ($-T\Delta S_{int}$) for each recombinant dimer combination (Table 4). These data are plotted in Figure 7, which illustrates the compensatory contributions of enthalpy and entropy as additional low-affinity interactions are added to the heterodimer. This plot also graphically illustrates that initiation of spectrin dimers is primarily enthalpically driven with a minor entropic contribution. That is, about 81% of the intrinsic Gibbs free energy driving α20−21 association with β1−2 arises from the intrinsic enthalpy change with $\Delta H_{int} = -8.6$ kcal/mol and $-T\Delta S_{int} = -2.0$ kcal/mol. In contrast, about 68% of the intrinsic Gibbs free energy driving α18−21 association with β1−4 comes from an intrinsic entropy change ($\Delta H_{int} = -3.5$ kcal/mol, $-T\Delta S_{int} = -7.3$ kcal/mol). Here, the cratic entropy is also a contributor to the intrinsic entropy. Murphy et al. suggest that the so-called cratic entropy is best described by the simple entropy of mixing (*34*). This leads to an estimated entropy decrease of 8 cal/(mol^{-1} K^{-1}) for bimolecular association as a unfavorable component. However, all binding reactions in this study involve a cratic entropy component, so the uncorrected intrinsic entropy changes are shown.

Enthalpic factors typically include van der Waals, hydrogen-bonding, and electrostatic interactions. A negative enthalpy

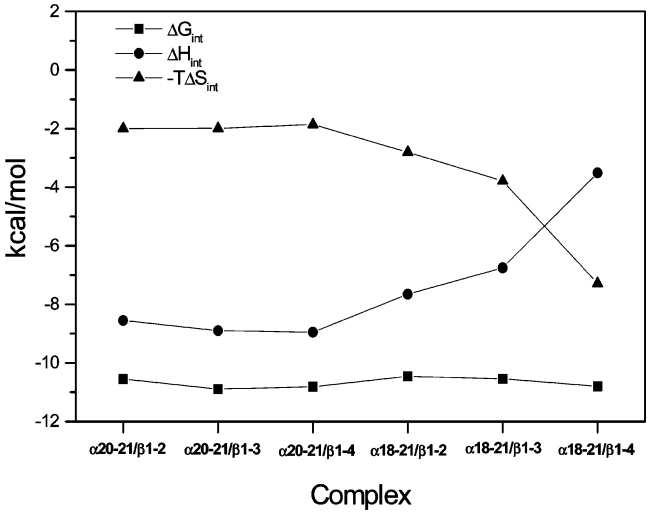

FIGURE 7: Changes in the intrinsic thermodynamic parameters. The intrinsic Gibbs free energy (ΔG_{int}), intrinsic enthalpy change (ΔH_{int}), and intrinsic entropy change (ΔS_{int}) were determined from data in Table 2 as described in the text and summarized in Table 4 for the various α/β dimers.

change often implicates hydrogen bonding as a substantial contributor to the strength of the interaction (*35*). Processes for which a positive entropy change is expected are the burial of electrostatic charges or hydrophobic groups. As the α20−21/β1−2 interaction is dominated by a favorable enthalpy change at 30 °C with a smaller favorable entropy component, dimer initiation apparently involves extensive hydrogen bond and salt bridge formation as well as a modest decrease in exposure of electrostatic charges or hydrophobic groups. This is consistent with previous studies using spectrin recombinant peptides and molecular modeling that suggested complementary electrostatic interactions played a key role in initial docking between complementary α and β motifs in the dimer initiation site (*15*). Furthermore, while intact dimers as well as two-motif and four-motif dimers could be weakened with increasing ionic strength buffers, the two-motif dimer was the most sensitive to increased ionic strength (*15*). Taken together, these observations suggest that the entropy contribution to dimer initiation is primarily due to burial of electrostatic groups used to correctly orient and dock the subunits. The substantial enthalpy contribution can be mainly attributed to extensive hydrogen bond formation with potential contributions from charge, van der Waals, and ion−dipole interactions.

It is very interesting that addition of a single low-affinity interaction (α19 ↔ β3) begins to shift the energetics toward an entropic process and addition of a second low-affinity interaction (α18 ↔ β4) continues this trend (Figure 7). When a positive entropic change dictates the magnitude of the Gibbs free energy, the interaction is probably dominated by hydrophobic interactions or burial of electrostatic interactions (*35*). The reduced sensitivity of a four-motif dimer to increased ionic strength compared with that of a two-motif dimer (*15*) suggests that weak, short-range, hydrophobic interactions predominate in lateral assembly of the motifs adjacent to the dimer initiation site.

As shown in Table 2 and Figure 7, the contributions of the two weak motif interactions to the K_d appear negligible when using ITC. Instead, the subtle increased overall affinity of low-affinity motif interactions are most easily demonstrated using competition assays (*8*, *12*, data not shown). In contrast, in a prior study we initially concluded that associations of weak interactions outside the dimer initiation site increased the binding affinity by about 5-fold per weak interaction (*11*). In this early study of dimer assembly, we used a relatively imprecise HPLC gel filtration binding assay to estimate the binding affinities of β peptides with α18−21, which yielded K_d values of about 230 nM for β1−2 association and 10 nM for β1−4 association. However, a subsequent study using ITC determined an average K_d of 14.2 nM for the β1−2 ↔ α20−21 interaction (*12*). The binding affinities observed in the current study are most consistent with the prior ITC experiments rather than the early HPLC binding assays. Specifically, when all experiments at pH 7.4 in the current study are considered, we observe an average K_d = 24.6 nM for β1−2 ↔ α20−21 with a range of 21.4−27.8 nM compared with an average K_d = 17.6 nM for β1−4 ↔ α18−21 and a range of 8.7−24.0 nM. It is clear from these comparisons that the gel-filtration-based estimate for the affinity of the four-motif interaction is consistent with more reliable subsequent ITC measurements, while the gel-filtration-based estimate for the two-motif interaction is weaker than in both subsequent ITC studies. There are two likely reasons for this discrepancy, which are probably related to each other. First, we previously observed that the α20−21 recombinants are very sensitive to mild oxidation and can readily form disulfide adducts with weak reducing reagents such as low concentrations of β-mercaptoethanol or glutathione. These adducts apparently interfere with dimer assembly (*12*). Second, if 10−20% of one reactant in a bimolecular association is inactivated (incompetent monomer) by either disulfide adduct formation or other factors, this will cause a substantial error in binding affinity estimates in a gel filtration assay. In contrast, the presence of 10−20% incompetent monomer in an ITC experiment will simply skew the observed stoichiometry, which typically ranges from 0.8 to 1.2 in 1:1 interactions due to small errors in protein concentrations as well as the presence of small amounts of incompetent monomer. In the current study, all spectrin recombinants were freshly purified for calorimetric measurements, and in some experiments, TCEP, a strong reducing reagent that cannot form adducts with cysteine residues, was used to ensure that all cysteines remained in the reduced state.

It is interesting that spectrin has a high density of both basic and acidic residues, yet only the α18/β4 interaction involves a protonation event. The pK values determined in this study are in good accordance with pK_a values typically observed for histidines involved in macromolecular complex formation (*36*, *37*). α18 has three histidines at positions 42, 52, and 72, whereas β4 has four histidines at positions 42, 55, 64, and 74 (Figure 8A). To see whether we could predict a likely candidate histidine that might be protonated during binding of α18 to β4, we constructed a model of an α18 ↔ β4 complex. The crystal structure of chicken brain spectrin α15−17 (PDB ID 1U4Q), with 53% sequence identity to α18 and 37% sequence identity to β4, was used as the template for building a homology model. The sequence alignment used for the model is shown in Figure 8A. The antiparallel dimer (Figure 8B) was constructed by application of structural superimposition with the crystal structure of the chicken brain α15 and α17 homodimer. According to the

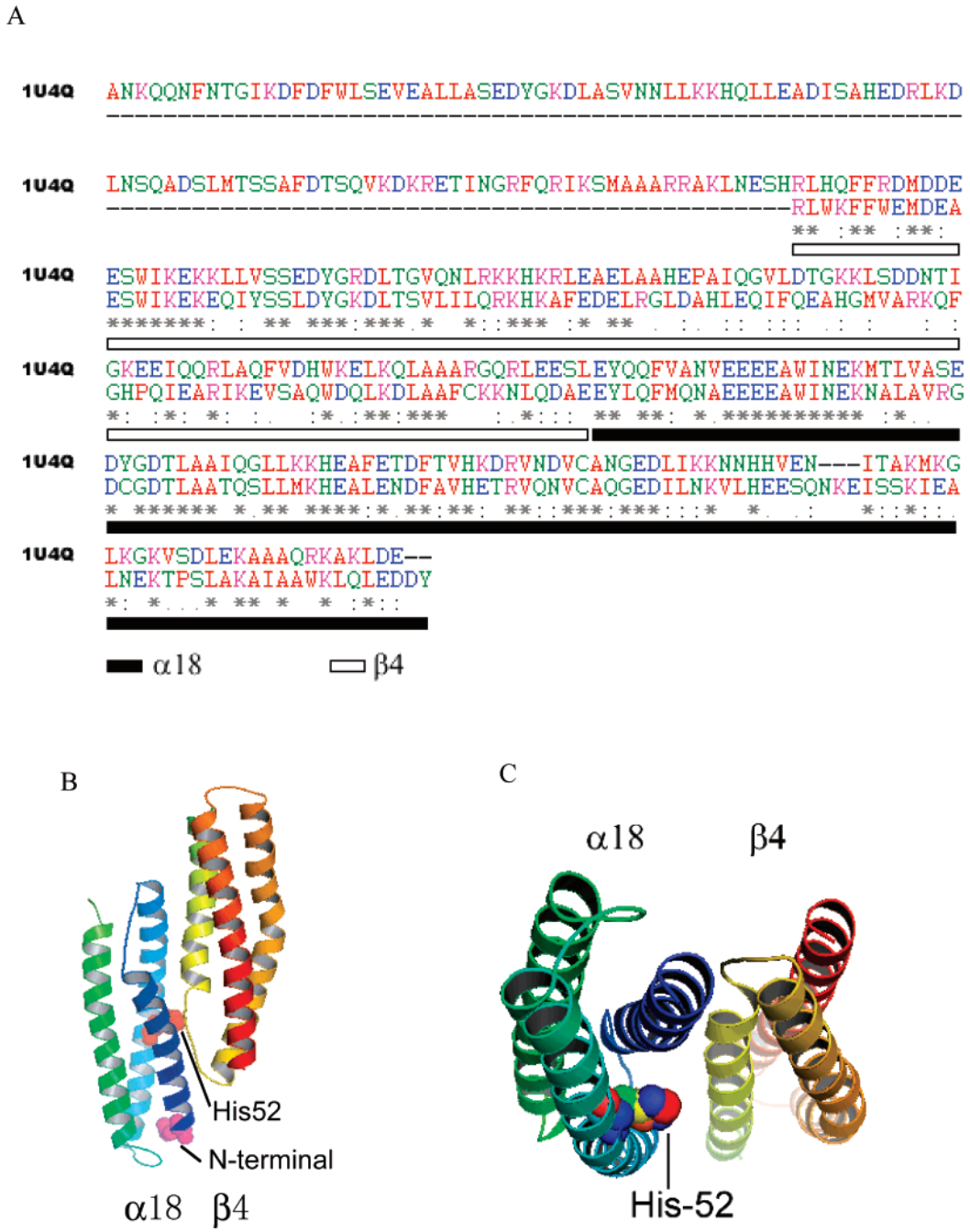

FIGURE 8: Model of the α18/β4 heterodimer: (A) target (α18 and β4) and template (chicken brain spectrin α15−17) sequence alignment, (B) model of the α18 and β4 heterodimer, (C) rotated orientation of the model with the α18 motif His52 side chain illustrated to show its proximity to the dimer interface.

Ramachandran plot, 95.5% of the residues of the α18/β4 heterodimer model are in the most favored region and no residues are found in disallowed regions. WhatCheck and the MODELLER DOPE command were also used to evaluate the current model (data not shown), and the results further support this as a good model. In this model, only the α18 His52 (Figure 8C) is located near the dimer binding site. We hypothesize that this residue may be primarily neutral in the monomer and become partially protonated upon dimer binding due to a conformational change in the environment of this residue that alters its p*K*. Although the α-amino group of α18 can be protonated at this pH, it does not lie close to the dimer interface region in our homology model (Figure 8B).

In summary, a detailed model of spectrin dimer assembly can be developed by integrating the results described above with prior observations from diverse studies. Two important points to consider are (1) both spectrin subunits have many tandem homologous three-helix-bundle motifs that can homodimerize with weak affinity, thereby demonstrating substantial promiscuity of monomeric chains, and (2) α-spectrin is synthesized in excess over β-chains. We therefore propose (1) a lock and key type unique register is initially provided by the high-affinity pairing of the β1−2 domain as the partially synthesized β-chain is emerging from the ribosome with α20−21 where correct alignment and docking is driven by long-range complementary electrostatic interactions, and as docking occurs, this interaction is stabilized

by hydrogen bonds and other hydrophilic interactions in a strongly exothermic association, and (2) adjacent complementary α and β motifs then sequentially pair, i.e., α19 ↔ β3, α18 ↔ β4, etc., in a process driven by a strong entropic component and an unfavorable enthalpic component. At least two questions that remain to be resolved are whether the weak lateral interactions are sequence specific or are merely driven by proximity to the dimer initiation site and whether the energetic processes involved in the two weak lateral pairs adjacent to the dimer initiation site apply to remaining weak lateral associations that propagate up the length of the dimer. Unfortunately, the latter question cannot be addressed using the experimental approach used in the current study because spectrin recombinants longer than approximately four motifs are sensitive to the shear forces in the ITC cell, leading to aggregation.

ACKNOWLEDGMENT

We thank Matthew Hart for performing the MALDI MS analyses and Emilie Gross for editorial assistance.

REFERENCES

1. Marchesi, V. T., and Steers, E. (1968) Selective solubilization of a protein component of the red cell membrane, *Science 159*, 203−204.
2. Clarke, M. (1971) Isolation and characterization of a water-soluble protein from bovine erythrocyte membranes, *Biochem. Biophys. Res. Commun. 45*, 1063−1070.
3. Fairbanks, G., Steck, T. L., and Wallach, D. F. H. (1971) Electrophoretic analysis of the major polypeptides of the human erythrocyte membrane, *Biochemistry 10*, 2606−2617.
4. Shotton, D. M., Burke, B. E., and Branton, D. (1979) The molecular structure of human erythrocyte spectrin−Biophysical and electron microscopic studies, *J. Mol. Biol. 131*, 303−329.
5. Speicher, D. W., and Marchesi, V. T. (1984) Erythrocyte spectrin is comprised of many homologous triple helical segments, *Nature 311*, 177−180.
6. Yan, Y., Winograd, E., Viel, A., Cronin, T., Harrison, S. C., and Branton, D. (1993) Crystal structure of the repetitive segments of spectrin, *Science 262*, 2027−2030.
7. Tang, H.-Y., and Speicher, D. W. (2004) In vivo phosphorylation of human erythrocyte spectrin occurs in a sequential manner, *Biochemistry 43*, 4251−4262.
8. Speicher, D. W., Weglarz, L., and Desilva, T. M. (1992) Properties of human red-cell spectrin heterodimer (side-to-side) assembly and identification of an essential nucleation site, *J. Biol. Chem. 267*, 14775−14782.
9. Wilmotte, R., Marechal, J., Morle, L., Baklouti, F., Philippe, N., Kastally, R., Kotula, L., Delaunay, J., and Alloisio, N. (1993) Low expression allele α^{LELY} of red cell spectrin is associated with mutations in exon 40 ($\alpha^{V/41}$ polymorphism) and intron 45 and with partial skipping of exon 46, *J. Clin. Invest. 91*, 2091−2096.
10. Wilmotte, R., Harper, S. L., Ursitti, J. A., Marechal, J., Delaunay, J., and Speicher, D. W. (1997) Exon 46-encoded sequence is essential for stability of human erythroid alpha-spectrin and heterodimer formation, *Blood 90*, 4188−4196.
11. Ursitti, J. A., Kotula, L., DeSilva, T. M., Curtis, P. J., and Speicher, D. W. (1996) Mapping the human erythrocyte β-Spectrin dimer initiation site using recombinant peptides and correlation of its phasing with the α-actinin dimer site, *J. Biol. Chem. 271*, 6636−6644.
12. Harper, S. L., Begg, G. E., and Speicher, D. W. (2001) Role of terminal nonhomologous domains in initiation of human red cell spectrin dimerization, *Biochemistry 40*, 9935−9943.
13. Viel, A., and Branton, D. (1994) Interchain binding at the tail end of the *Drosophila* spectrin molecule, *Proc. Natl. Acad. Sci. U.S.A. 91*, 10839−10843.
14. Viel, A., Gee, M. S., Tomooka, L., and Branton, D. (1998) Motifs involved in interchain binding at the tail-end of spectrin, *Biochim. Biophys. Acta 1384*, 396−404.
15. Begg, G. E., Harper, S. L., Morris, M. B., and Speicher, D. W. (2000) Initiation of spectrin dimerization involves complementary electrostatic interactions between paired triple-helical bundles, *J. Biol. Chem. 275*, 3279−3287.
16. Law, R., Harper, S. L., Speicher, D. W., and Discher, D. E. (2004) Influence of lateral association on forced unfolding of antiparallel spectrin heterodimers, *J. Biol. Chem. 279*, 16410−16416.
17. Riahi, M. H., Kakhniashvili, D. G., and Goodman, S. R. (2005) Ubiquitination of red blood cell α-spectrin does not affect heterodimer formation, *Am. J. Hematol. 78*, 281−287.
18. Goodman, S. R., Pace, B. S., and Shartava, A. (1999) New therapeutic approaches to sickle cell disease: Targeting RBC membrane oxidative damage, *Cell. Mol. Biol. Lett. 3*, 403−411.
19. Monterio, C. A., Gibson, X. A., Shartava, A., and Goodman, S. R. (1998) Preliminary characterization of a structural defect in homozygous sickle cell a-spectrin demonstrated by a rabbit autoantibody, *Am. J. Hematol. 58*, 200−205.
20. Sangerman, J., Kakhniashvili, D., Brown, A., Shartava, A., and Goodman, S. R. (2001) Spectrin ubiquitination and oxidative stress: potential roles in blood and neurological disorders, *Cell. Mol. Biol. Lett. 6*, 607−636.
21. Grum, V. L., Li, D. N., MacDonald, R. I., and Mondragon, A. (1999) Structures of two repeats of spectrin suggest models of flexibility, *Cell 98*, 523−535.
22. Kusunoki, H., Minasov, G., MacDonald, R. I., and Mondragon, A. (2004) Independent movement, dimerization and stability of tandem repeats of chicken brain α-spectrin, *J. Mol. Biol. 344*, 495−511.
23. Kusunoki, H., MacDonald, R. I., and Mondragon, A. (2004) Structural insights into the stability and flexibility of unusual erythroid spectrin repeats, *Structure 12*, 645−656.
24. Djinovic-Carugo, K., Young, P., Gautel, M., and Saraste, M. (1999) Structure of the α-actinin rod: Molecular basis for cross-linking of actin filaments, *Cell 98*, 537−546.
25. Ylanne, J., Scheffzek, K., Young, P., and Saraste, M. (2001) Crystal structure of the α-actinin rod reveals an extensive torsional twist, *Structure 9*, 597−604.
26. Wiseman, T., Williston, S., Brandts, J. F., and Lin, L. N. (1989) Rapid measurement of binding constants and heats of binding using a new titration calorimeter, *Anal. Biochem. 179*, 131−137.
27. Arnold, K., Bordoli, L., Kopp, J., and Schwede, T. (2006) The SWISS-MODEL workspace: a web-based environment for protein structure homology modeling, *Bioinformatics 22*, 195−201.
28. Sali, A., and Blundell, T. L. (1993) Comparative protein modeling by satisfaction of spatial restraints, *J. Mol. Biol. 234*, 779−815.
29. Chenna, R., Sugawara, H., Koike, T., Lopez, R., Gibson, T. J., Higgins, D. G., and Thompson, J. D. (2003) Multiple sequence alignment with the Clustal series of programs, *Nucleic Acids Res. 31*, 3497−3500.
30. Laskowski, R. A., MacArthur, M. W., Moss, D. S., and Thornton, J. M. (1993) PROCHECK: a program to check the stereochemical quality of protein structures, *J. Appl. Crystallogr. 26*, 283−291.
31. DeLano, W. L. (2004) *The PyMOL molecular graphics system user's manual*, DeLano Scientific, San Carlos, CA.
32. Bates, R. G., and Hetzer, H. B. (1961) Dissociation constant of protonated acid form of 2-amino-2-(hydroxymethyl)-1,3-propanediol [tris-hydroxymethyl)-aminomethane] and related thermodynamic quantities from 0 to 50°, *J. Phys. Chem. 65*, 667−671.
33. Baker, B. M., and Murphy, K. P. (1996) Evaluation of linked protonation effects in protein binding reactions using isothermal titration calorimetry, *Biophys. J. 71*, 2049−2055.
34. Murphy, K. P., Xie, D., Thompson, K. S., Amzel, L. M., and Freire, E. (1994) Entropy in biological binding processes−estimation of translational entropy loss, *Proteins 18*, 63−67.
35. Winzor, D. J., and Sawyer, W. H. (1995) *Quantitative characterization of ligand binding*, pp 1−2, John Wiley and Sons, Inc., New York.
36. Jacobson, T., Williamson, J., Wasilewski, A., Felesik, J., Vitello, L. B., and Erman, J. E. (2004) Azide binding to yeast cytochrome c peroxidase and horse metmyoglobin: comparative thermodynamic investigation using isothermal titration calorimetry, *Arch. Biochem. Biophys. 422*, 125−136.
37. Pierce, M. M., Raman, C. S., and Nall, B. T. (1999) Isothermal titration calorimetry of protein-protein interactions. *Methods 19*, 213−221.

BI7007905